Cerebral Cortex Advance Access published April 8, 2010

Cerebral Cortex
doi:10.1093/cercor/bhq059

The Neural Processes Underlying Self-Agency

Fatta B. Nahab[1,2], Prantik Kundu[1,2], Cecile Gallea[2], John Kakareka[3], Randy Pursley[3], Tom Pohida[3], Nathaniel Miletta[2], Jason Friedman[4] and Mark Hallett[2]

[1]Department of Neurology, University of Miami, Miller School of Medicine, Miami, FL 33136, USA, [2]Human Motor Control Section, Medical Neurology Branch, National Institutes of Neurological Disorders and Stroke, [3]Signal Processing and Instrumentation Section, Division of Computational Bioscience, Center for Information Technology, National Institutes of Health, Bethesda, MD 20892, USA and [4]Department of Computer Science and Applied Mathematics, Weizmann Institute of Science, Rehovot 76100, Israel

Address correspondence to Fatta B. Nahab, MD, Department of Neurology, University of Miami, Miller School of Medicine, Clinical Research Building (C-215), 1120 Northwest 14th Street, Suite 1347, Miami, FL 33136, USA. Email: fnahab@med.miami.edu.

Self-agency (SA) is the individual's perception that an action is the consequence of his/her own intention. The neural networks underlying SA are not well understood. We carried out a novel, ecologically valid, virtual-reality experiment using blood oxygen level–dependent functional magnetic resonance imaging (fMRI) where SA could be modulated in real-time while subjects performed voluntary finger movements. Behavioral testing was also performed to assess the explicit judgment of SA. Twenty healthy volunteers completed the experiment. Results of the behavioral testing demonstrated paradigm validity along with the identification of a bias that led subjects to over- or underestimate the amount of control they had. The fMRI experiment identified 2 discrete networks. These leading and lagging networks likely represent a spatial and temporal flow of information, with the leading network serving the role of mismatch detection and the lagging network receiving this information and mediating its elevation to conscious awareness, giving rise to SA.

Keywords: efference copy, fMRI, ownership, sense of agency, voluntary movement

Introduction

As humans, we normally sense that we are the agents of our own actions. This perception is referred to as self-agency (SA; Gallagher 2000). An individual's SA is considered intact when 2 conditions are met. First, the agent must perceive ownership over an effector. The effector is usually a body part, though some experimental paradigms have successfully created the illusion of self-ownership over an artificial hand (Costantini and Haggard 2007). Second, the sensory consequences of an effector's actions must match the intentions of the agent. When both conditions are true, the agent plans an action that is subsequently performed by the effector and thereby reinforces the individual's SA. In circumstances where the action does not match the intention, or an action is not preceded by the intention, a mismatch is detected and would evoke the sense of movement without agency, an involuntary movement. The ability to monitor SA has been suggested as a means by which to distinguish self from other in the environment (Frith 1992). Although the agent has the ability to explicitly judge whether ownership and SA are present, this process usually occurs at preconscious levels outside of the agent's awareness (Jeannerod 1997; Synofzik et al. 2008). In real-life situations, only after a loss of SA is detected does the agent become aware of the incongruency (Slachevsky et al. 2001).

The neural correlates of SA have been studied extensively in various experiments, most of which manipulate the explicit or implicit judgment of SA by experimental subjects through the introduction of spatial or temporal delays to simulate mismatches between intention, action, and sensory feedback (for a review, see David et al. 2008). Regions showing increased activation with loss of SA include motor areas such as ventral premotor cortex; the supplementary motor area (SMA and pre-SMA); and the cerebellum along with the posterior parietal cortex (PPC), posterior superior temporal sulcus (STS), and the insula (Fink et al. 1999; Haggard and Magno 1999; Farrer and Frith 2002; Farrer et al. 2003; Leube et al. 2003; Ehrsson et al. 2004; Sirigu et al. 2004; Karnath et al. 2005; Brass and Haggard 2007; Klein et al. 2007; Repp and Knoblich 2007). Despite the broad network implicated in SA, little is known about the specific function of these regions in SA and, more importantly, the character of their connectivity (David et al. 2007). Experimental paradigms also had limited ecological validity since they imposed binary outcomes to what is likely a complex and dynamic cognitive process.

To further characterize the neural mechanisms underlying SA, we designed a novel, ecologically valid virtual-reality paradigm where SA could be modulated in real time while subjects performed voluntary finger movements. While performing the task, we measured implicit judgment of SA with blood oxygen level–dependent (BOLD) functional magnetic resonance imaging (fMRI) and explicit judgment during a behavioral study. We hypothesized that regions previously implicated in monitoring SA would demonstrate a differential response and connectivity pattern based on the level of control experienced.

Materials and Methods

Subjects

Healthy volunteers were recruited from the local community for participation in this study. All subjects underwent general medical screening, neurological testing, and a clinical MRI to exclude latent structural lesions. Subjects were also excluded if they had abnormalities on neurological examination, were pregnant, taking centrally active medications, or had a contraindication for undergoing MRI. Subjects were also instructed to abstain from caffeine and alcohol for 48 h prior to scanning. All subjects provided written informed consent in compliance with the Institutional Review Board of the National Institute of Neurological Disorders and Stroke.

Overview of Stimulus Paradigm

The stimulus paradigm was based on a quantitative modulation of SA. To modulate SA during fMRI, we developed an adaptive motor

paradigm. Subjects performing voluntary sequential finger movements received real-time visual feedback from a simulated hand displayed on a screen. The simulated hand displayed the subject's movements in near real time (<50 ms lag). We used a Cyberglove (Cyberglove Systems) 18-sensor data glove to record subject finger movements during the paradigm.

SA was modulated using a computerized adaptive motor paradigm that varied the movement response by the simulated hand between 100% control (subject movements driving the simulation entirely) and 0% control (prerecorded movement data driving the simulation entirely). Intermediate levels of control included 25%, 50%, and 75% along with 2 control conditions consisting of subjects watching a moving hand (W condition) and moving without visual feedback (M condition; see Fig. 1).

The stimulus display, modulation methods, and recordings were carried out using software written in-house using C++ and drivers provided by Cyberglove Systems. The graphical user interface was written using the wxWidgets open source framework and utilizes OpenGL drivers for the 3D graphics.

Customized Data Glove Calibration

To ensure that each subject felt a sense of ownership over the projected simulated hand, we calibrated each subject's individual finger movements to compensate for subtle differences in how the glove may fit a particular subject's hand. We created a custom calibration program using methods developed by Friedman (2007) to provide a precise representation of the hand movements. Calibration procedures were conducted at baseline and before fMRI. Calibration optimization was carried out until a subject endorsed the feeling that the simulated hand was an extension of their own body and under their full control.

Training/Experiment

After calibration procedures were completed, subjects performed practice sessions to ensure consistent performance and the development of a sense of ownership over the simulated hand. The movement subjects performed consisted of individual finger flexion then extension starting with the fifth finger, moving sequentially toward the second finger and going back (5-4-3-2-3-4-5-4 . . .). The use of the thumb was excluded from the sequence. Subjects were trained to perform 4 different tasks based on the character displayed on the screen. A "+" signified visual fixation during which time subjects were to avoid any limb movements, an "m" signified the subject should perform the finger sequence without receiving visual feedback as long as the "m" was displayed, and a "w" displayed for 1 s signified the subject should passively watch the subsequent simulated hand moving while maintaining their own hand at rest. Lastly, the task of primary interest was to perform the sequential finger movements at a consistent pace whenever the simulated hand was projected on the screen. For this condition (% control), subjects were instructed to perform the movements while viewing the simulated hand. For subjects to remain naive to the modulation of SA, they were informed that "the hand on the screen may not always do what you intend, but you should continue to perform your finger movements." These instructions were intended to address observations we made during the development phase of this paradigm showing that subjects during the 25% control condition could sometimes be seen to follow the simulation rather than continue their own internally generated movements. Thus, we wanted to ensure that subjects did not artificially raise their level of SA by following rather than leading. We also provided no explanation of how this modulation would take place or whether there would be different levels of modulation. All movements were monitored online and were also saved at the completion of each run. This allowed the investigator to playback the motions and ensure proper task performance.

Scan Summary

Subjects were positioned in the MRI to ensure that the head was adequately constrained to minimize head motion. The gloved right hand was positioned out of the subject's field of view and was touching neither the subject nor the MRI since this could diminish the sense of ownership. The images were projected onto a screen, viewed using a mirror mounted on the head coil, providing subjects with a full field

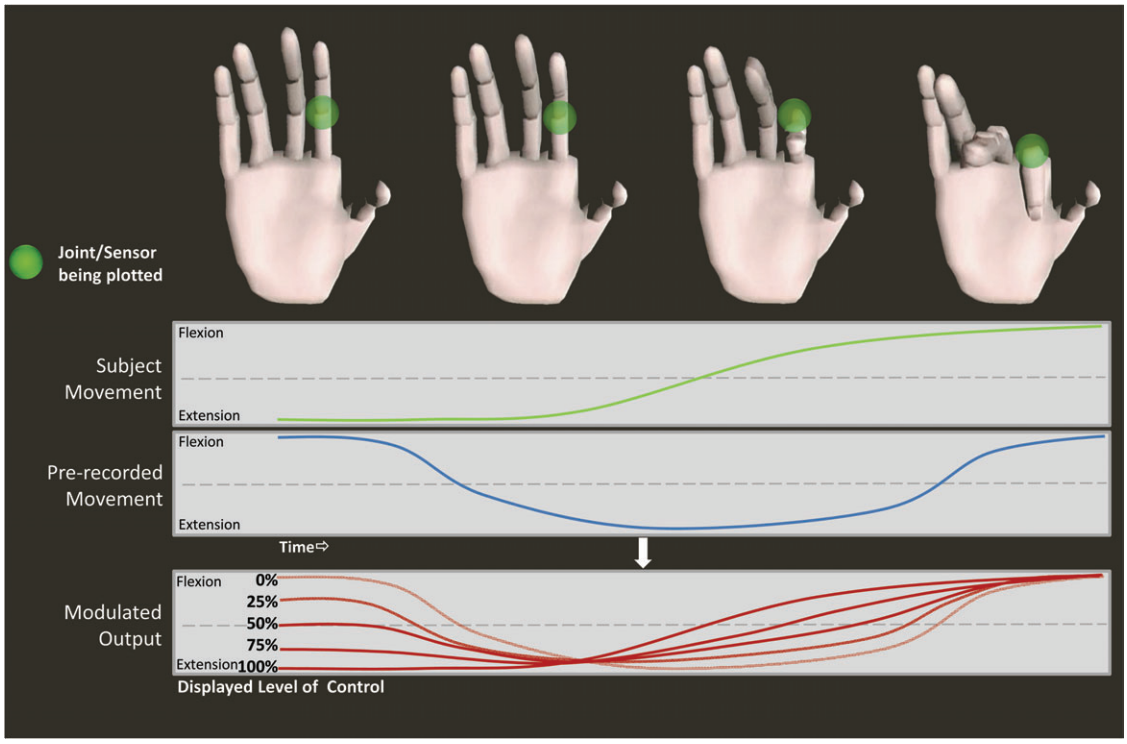

Figure 1. Demonstration of virtual-reality paradigm showing the joint angle data from one of 18 total sensors while the subject performs the sequential finger movements. The level of SA is modulated based on the relative contribution of the subject's actual data with a prerecorded set of movements to produce the output of the model hand seen by the subject. Note the actual paradigm performs these calculations for all 18 sensors simultaneously.

of view. There were seven possible conditions: 100% control, 75%, 50%, 25%, 0%, move, and watch. Each stimulus was presented as a 20-s block separated by 20 s of visual fixation to allow the hemodynamic response to return toward baseline. Each condition was pseudorandomly repeated 5 times over the course of 5 runs. Each run lasted for 310 s. Run order was randomly varied across subjects to avoid stimulus sequence interactions. The total MRI acquisition time per subject was approximately 50 min.

Image Acquisition

Structural and functional images were acquired with a 3-T MRI scanner (Signa, General Electric) using a GE 8-channel head coil. BOLD fMRI data were acquired using a gradient-echo echo-planar pulse sequence and GE ASSET parallel imaging technique (64 × 64 matrix, repetition time [TR] = 2000 ms, time to echo [TE] = 30 ms, field of view [FOV] = 22 cm, flip angle [FA] = 70°, ASSET factor = 2). Whole-brain coverage was obtained with 40 axial slices (3.2 mm thickness, 0.3 mm spacing, in-plane resolution = 3.44 × 3.44 mm). A total of 150 echoplanar image (EPI) volumes were acquired for each of the 5 runs. The first 5 volumes of each run, collected before equilibrium magnetization was reached, were discarded prior to analysis. High-resolution anatomical images (128 axial slices, 1.3 mm thickness, in-plane resolution = 0.94 × 0.94 mm) were obtained using a standard magnetization-prepared rapid gradient echo (MP-RAGE) sequence (256 × 256 matrix, TR = 6.172 ms, TE = 3.22 ms, FOV = 24 cm, phase FOV = 0.81, FA = 10°) to serve as an anatomical reference for spatial normalization.

Behavioral Testing

At the completion of the scan sessions, subjects were taken outside the scanner to perform a sixth run consisting of 2 repetitions each of the 5 levels of control, displayed pseudorandomly, for a total of 10 blocks. Subjects were instructed to perform the same sequential finger movements as during the fMRI session while viewing a computer monitor at a natural distance in front of them and concealing their forearms under the computer table. At the completion of each block, subjects were asked to "report the level of control experienced over the simulated hand, rating anywhere from 0% (no control) to 100% (full control)."

Data Analysis

Image processing and analysis were performed with the AFNI software package (Cox 1996; Saad et al. 2006). The EPI and anatomical data sets were converted from DICOM format to AFNI's native 3D and 4D formats. EPI time series data were corrected for slice timing offset. A 6-parameter rigid body inter- and intrasession motion correction was performed whereby volumes in the EPI scans were registered to the last EPI volume collected prior to the high-resolution MP-RAGE scan. EPI time series data were smoothed using a 6-mm full width at half-maximum isotropic Gaussian kernel to minimize the anatomical variability among individual subject maps in generating group maps. The data were scaled by dividing voxel signal intensity by the mean voxel intensity for each session and multiplying the result by 100. The resulting regression coefficients thus represent a percent signal change from the mean. The 3D anatomical and 4D time series data sets were then transformed to Talairach–Tournoux standard space with a resolution of 3 × 3 × 3 mm^3.

To model the hemodynamic response functions for linear regression analysis, we convolved the timing of each stimulus class with a gamma-variate function that approximated the BOLD response (Cohen 1997). For each voxel, the fixed shape analysis resulted in a single response amplitude for each stimulus class. In addition to the regressors that modeled the stimulus response, we included regressors to model motion residuals and baseline drifts using quadratic polynomials in time for each run. The statistical correction for multiple comparisons was set by rejecting spatial clusters smaller than what would be expected by chance using Monte-Carlo simulations (Forman et al. 1995), given a voxel-wise false-positive level of $P < 0.001$ that resulted in a corrected $P < 0.05$ (minimum cluster size of 13 voxels, 351 μL).

For the group analysis, we analyzed individual subject regression coefficients using a 2-way analysis of variance (ANOVA) with the 7-stimulus classes as fixed effects and subject as random effects. This analysis is also commonly termed a 1-way within-subject ANOVA.

Connectivity Analysis

After regions featuring the leading and lagging responses were identified, a relationship between the networks of the leading and lagging responses was sought. This was evaluated with a seed correlation analysis (SCA), a form of functional connectivity analysis. SCA involves the regression of every voxel time course of an individual subjects' brain to a model including one or more reference time courses with general linear model multiple regression. The reference time courses chosen for each subject were from voxels of the subject's own brain, but the location of voxels from which time courses were extracted was determined from group analysis. As the relationship between the leading and lagging networks were in consideration, a multiple regression involving 2 regressors of interest was executed for each subject. One regressor was from the location of peak loss response in the inferior parietal lobule (IPL), since the group average time course suggested its activity to be most representative of the lagging response (see results of 2-way ANOVA). The other was from the peak in the superior temporal gyrus, since this region was considered most representative of the leading response.

For each subject, the regressors were extracted from the individual subjects' brains after motion parameters, and drift effects were removed using base regression. The regression analysis was executing using the 3dDeconvolve tool from the AFNI analysis package. The multiple regression analysis provides partial correlation regression coefficients for each regressor included in the regression model. Each correlation coefficient quantifies the particular contribution of the respective regressor to the total time course, exclusive of the others included in the model. This indicates that if a voxel's total time course is predominantly represented by one regressor, regardless of that regressors' qualitative similarity to another regressor (within a maximum similarity), then the correlation coefficient of that regressor will far outweigh that of the other. If, however, the correlation coefficients of both regressors are similar or equivalent to each other, then it is indicated that both regressors contribute to the time course equivalently (at a provided confidence interval). Every voxel's correlation coefficient for a particular regressor is represented in a volumetric SPM for each subject. All individual subject SPMs are then inputted into a volumetric one-sample *t*-test to obtain a group analysis of the network corresponding the each response type. The result was 2-group SPMs, each representing the network corresponding to a response type. Each group SPM was thresholded at the cluster alpha value of 0.05 (Bonferroni multiple comparisons correction). The maps were then graphically overlaid to produce a conjunction analysis showing intensity effects.

Technical Issues Relating to Use of Cyberglove in MR Environment

When used in an MRI environment, the Cyberglove system is susceptible to 2 dominant noise sources. The first noise source corresponds to the radio-frequency excitation pulse and causes single-point errors in the Cyberglove sensor data. The resulting visual effects on the 3D rendered hand are quick, unnatural movements in one or more joints of the hand. A 5-tap median filter was applied to each sensor to minimize this type of spike error. An *n*-tap median filter takes *n* consecutive samples centered at the current time point (i.e., sample), sorts them in increasing order, and uses the middle (assuming *n* is an odd number) sample to replace the current sample point. The second noise source corresponds to the MRI gradient coils that generate spurious currents in the Cyberglove strain gauge sensors and/or cable leading from the glove. The resulting visual effect on the 3D rendered hand is uncontrollable shaking. Prior to reconstruction of the visual feedback, a low-pass digital filter is applied to each sensor data to minimize the appearance of shaking. The filter used is a 21-tap Kaiser Filter with a cutoff of 2 Hz and a beta of 2.024. The filter parameters were empirically derived during system testing to eliminate the

majority of shaking without adversely affecting the display of actual hand motions. The median filter is applied before the low-pass filter to prevent the large noise spikes from affecting the low-pass filter.

Results

Behavioral Data

Twenty healthy right-handed subjects (18–33 years of age, mean age 23.3, 10 females) provided written informed consent and participated in this study. The validity of the paradigm was assessed across the group by 2 measures. First, the intersubject repeatability was determined by calculating the standard deviation (SD) of subject-reported SA. Additionally, the ability of subject-reported SA levels to accurately reflect objective levels of percent control was determined by calculating the mean reported SA at each level of control (see Fig. 2). The SDs across the different levels of control showed greatest intersubject variability at 50% control and least variability at 100% control. Mean SA ratings were within 15% of the actual control level for each condition. At higher levels of control (50% and 75%), SA ratings overestimated control to be 66% and 90%, respectively, while the 25% control condition was underestimated as 16%. The 100% and 0% conditions were both within 5% points of the actual value. Based on these findings, subjects were able to explicitly judge their level of agency reliably during the behavioral task.

fMRI Data

In contrast to the measurement of explicit judgment of SA during the behavioral experiment, the fMRI experiment sought to identify the neural correlates during the implicit monitoring of different levels of SA. A review of the subject movements during the experiment showed subjects generally performed the task as directed, with maintenance of the sequential figure movements despite periods where control was lost and minimal head motion (mean ± SD: 0.27 ± 0.30 mm, range: 0.1–1.2 mm). Although it is possible that some subjects made explicit judgments during the fMRI experiment, we have no information to suggest this. The maps generated by the linear trend map method served to consolidate the BOLD responses from every condition into a concise visualization. This allowed us to differentiate between regions that responded similarly across all tasks and could be obtained by standard parametric contrasts, as compared with brain regions that were uniquely sensitive to changes in the level of SA. Based on the LTM analysis, we identified regions whose BOLD responses were linearly proportional to the loss of SA (Fig. 3). We found no regions that demonstrated linearly increasing BOLD responses during the gain of control, though a number of expected regions such as primary sensorimotor and occipital cortices showed task-sustained activity with no proportionality to the level of control experienced.

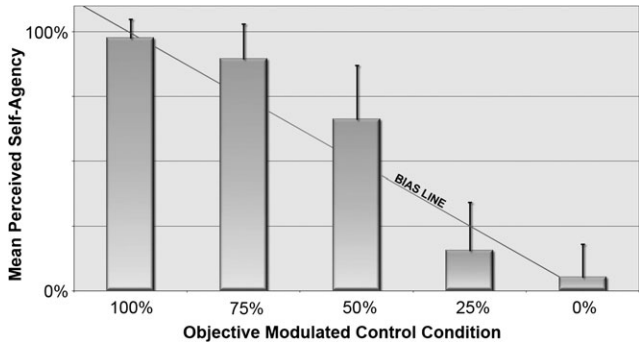

Figure 2. Results of the behavioral experiment showing the group mean perceived level of SA for each objective level of control (error bars = SD). Line represents the point where SA matches the objective level of control provided by the paradigm. Subject report of SA was highly consistent and demonstrated a bias toward greater SA at the 50% or greater control and a bias toward less SA at 25% control.

To confirm the presence or absence of response proportionality to the level of SA, we studied the group time courses of regions showing nonproportional task responsivity and those of loss-responsive regions. Regions with a nonproportional task response included areas such as primary sensorimotor cortex (hand knob; $x = -32$, $y = -32$, $z = 51$) and middle occipital cortex ($x = 33$, $y = -84$, $z = -1$). The time courses for these regions had a typical sustained hemodynamic response characteristic of block design paradigms (see Fig. 4). The individual time courses for the 0–75% control conditions are indistinguishable, while the 100% control condition shows slightly lower amplitude. The watch and move conditions have distinctly lower response amplitudes that are consistent with the regions of interest.

Loss-responsive regions featured hemodynamic characteristics of a radically different nature from those with nonproportional task responsivity (see Fig. 5). The time courses of each loss-responsive region are all of consistent character and distinguishable only by a scaling factor that is inversely proportional to the percentage of control provided by the respective condition. The 0% condition consistently had the highest amplitude, and the 100% condition had the least. The watch and move conditions evoked hemodynamic profiles of completely different character and generally lower level BOLD responses. All loss-responsive regions also showed hemodynamic responses belonging to one of 2 classes of phasic activity, referred to here as "leading" and "lagging" responses. Table 1 summarizes the loss-responsive regions and whether their BOLD response was of a leading or lagging type. Leading-response regions feature a hemodynamic peak within 4-s of stimulus onset and a persistent high-amplitude phase lasting another 4 s. This is followed by a low-amplitude period and then a second amplitude peak at 14 s after stimulus onset that is of lower amplitude than the first. Finally, a third large peak occurs at 24 s, which coincides with task completion and a subsequent return to baseline. Lagging response regions are characterized by a slightly later peak than that seen during the leading response, occurring at 4 to 6 s following stimulus onset, and a slow return to baseline with progressively lower amplitude phases.

To determine whether the leading and lagging regions comprised discrete, yet connected, functional networks, we performed a seed-based correlation analysis based on the regions identified by the loss-responsive LTM peaks. Our findings revealed that these 2 response groups, leading and lagging, functioned coherently in 2 distinct networks spanning frontal, temporal, and parietal cortices (see Fig. 6). Additional regions anatomically intermediate to leading and lagging networks appeared to serve as a relay between the 2 functional networks. This was evidenced by their high correlation values to both networks. Relay areas were present in the bilateral prefrontal cortex, bilateral PPC, bilateral basal ganglia, precuneus, right STS, and left cerebellar hemisphere.

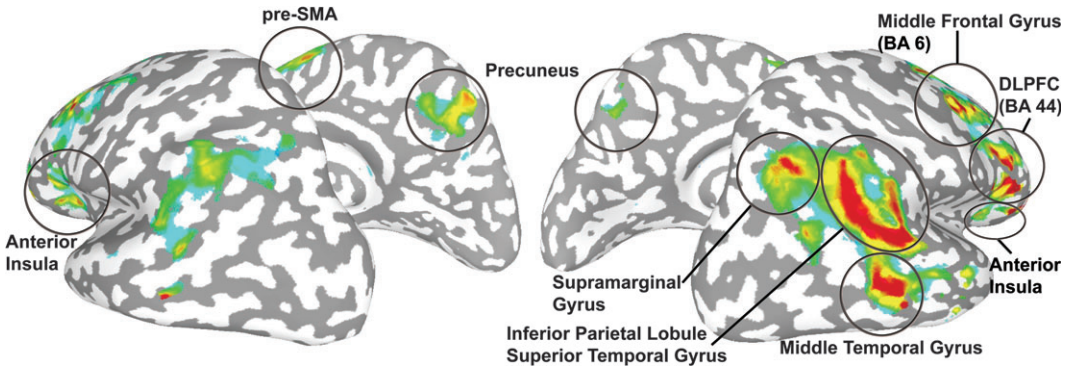

Figure 3. Linear trend map of regions responding proportionally to the loss of SA displayed on an inflated standard brain ($P = 0.05$, corrected). The response to the loss of SA was mediated by bilateral brain regions, though the right hemisphere produced preferentially larger and more proportional responses.

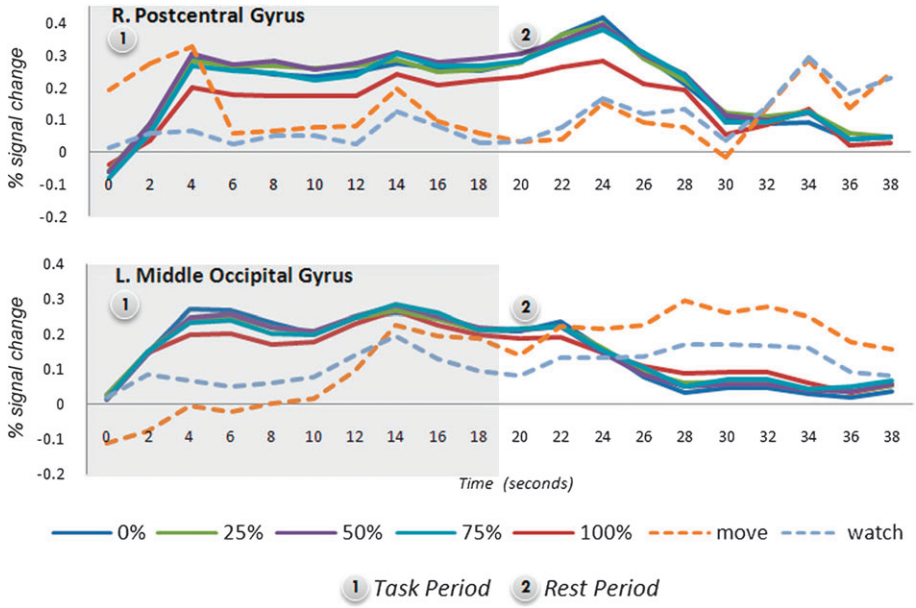

Figure 4. Mean BOLD response time courses for primary sensorimotor and middle occipital cortices. These regions showed a nonproportional task response to the modulation of SA. The hemodynamic response function (HRF) for the move control condition was greatest in the motor region, while the HRF for the watch control condition was of a greater magnitude in the visual cortex. The 100% control condition was associated with a slightly smaller HRF than the remaining levels of control, though the 0–75% conditions could not be differentiated from one another.

Discussion

Elucidating the neural elements and mechanisms that generate the sense of agency has been a topic of introspection and study since the time of James (1890). The earliest physiological explanations of SA are based on a classical "comparator" model. This theory postulates that separate information streams relating to motor planning and sensory feedback from the effector are directed to a specialized brain region that compares the streams for congruence, with a mismatch between intention and sensory feedback suggesting external generation (Sperry 1950; Von Holst 1954; Frith et al. 2000). Synofzik et al. (2008) have elegantly argued that SA or the explicit judgment of SA cannot be adequately explained solely by a mismatch detection system. This case can be illustrated in patients with parietal lobe injury experiencing impaired mismatch detection, yet still maintaining SA (Sirigu et al. 1999). Instead, the parietal mismatch detection system may contribute to the processing of SA that is hypothesized to occur in a higher cortical center, such as prefrontal cortex (Fink et al. 1999; Slachevsky et al. 2001). This would ultimately be the region responsible for the experience of SA at a conscious level.

Two aspects of the human perception and processing of SA were assessed in our joint behavioral and fMRI experiments, utilizing a paradigm that simulated the loss of SA in virtual reality. We were aware of the critical importance of fostering a sense of self ownership and control in order to properly study SA. This led to the rigorous multistage calibrations described in the methods section. The results of our combined fMRI and behavioral study provide new insights into the neural mechanisms underlying SA.

The behavioral study provides several important findings. First, a validation of our novel, ecologically valid, virtual-reality paradigm showing that subjects could reliably judge SA with little intersubject variability. Second, that intermediate levels of SA may be experienced, suggesting that at least the judgment of SA is not a binary perception. Finally, it provides a further

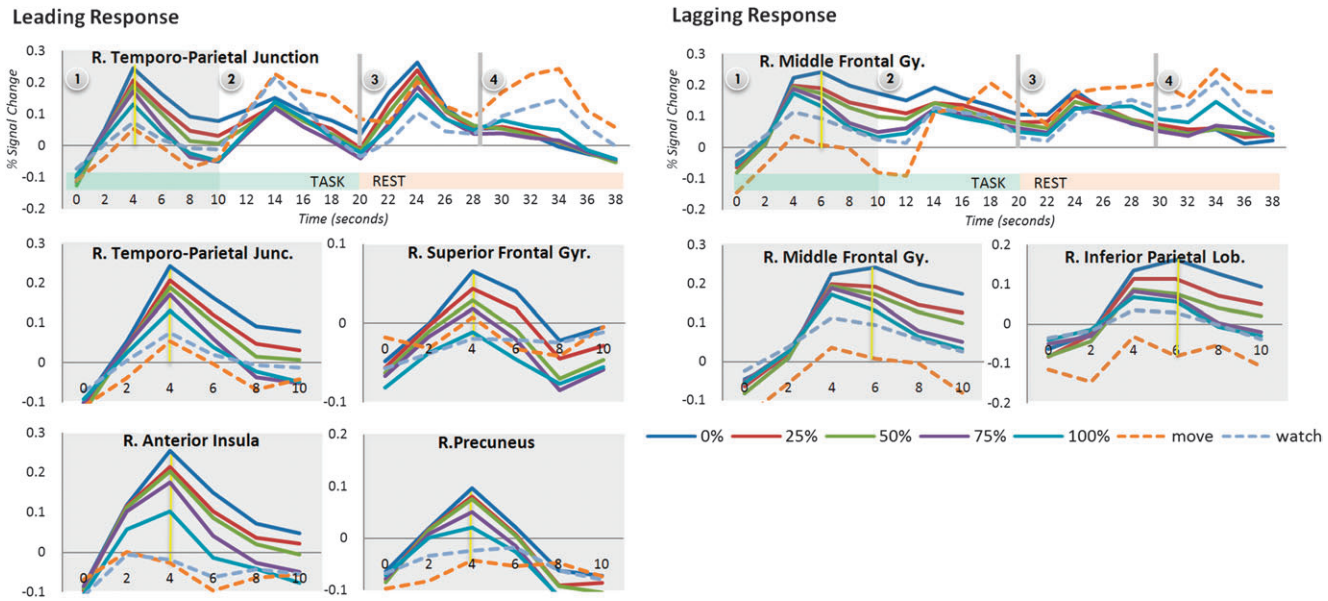

Figure 5. Mean BOLD response time courses for regions showing proportional responsivity to the level of control as SA were lost. The hemodynamic response functions for these loss-responsive regions showed either of 2 response profiles: leading or lagging. Leading regions showed response peaks at 4, 14, and 24 s after stimulus onset, while lagging regions showed more subtle peaks and a slower return to baseline.

Table 1
Summary of loss-responsive brain regions

Region	Coordinates			*t*-value
	x	*y*	*z*	
Leading-response regions				
Right superior temporal gyrus	56	−50	12	7.293
Right superior temporal gyrus	52	−46	18	7.1
Right superior frontal gyrus	20	8	56	6.172
Right middle temporal gyrus	62	−50	6	6.098
Right middle frontal gyrus	22	8	62	5.333
Right superior temporal gyrus	40	−46	14	5.094
Right supramarginal gyrus	58	−52	36	5.073
Left inferior parietal lobule	−50	−52	44	4.989
Left cerebellar tonsil	−38	−56	−40	4.926
Right middle frontal gyrus	32	2	54	4.844
Left insula (anterior)	−32	20	2	4.692
Right precuneus	8	−56	42	4.458
Left middle frontal gyrus	−38	46	24	4.441
Right angular gyrus	34	−58	36	4.438
Left insula (anterior)	−34	16	12	4.409
Right insula (anterior)	21	20	5	4.389
Right superior temporal gyrus	50	−56	24	4.326
Right middle frontal gyrus	40	26	42	4.294
Right middle frontal gyrus	38	10	32	4.257
Right middle temporal gyrus	52	−40	−4	4.146
Right superior frontal gyrus	8	8	54	4.102
Lagging-response regions				
Right inferior parietal lobule	46	−62	38	5.855
Right inferior parietal lobule	46	−56	50	5.057
Left inferior parietal lobule	−44	−50	38	4.569
Right middle frontal gyrus	44	8	54	4.464
Left cerebellar pyramid	−14	−70	−28	3.958
Left middle frontal gyrus	−46	40	18	3.93

Note: The regions are separated, based on the hemodynamic profile, into leading and lagging response types.

dissociation of the SA intrinsic bias that previous authors have described (Wegner et al. 2004; Synofzik et al. 2006). Results of the present study revealed that the level of SA across conditions had a sigmoidal relationship to the actual level of control. The complete presence or absence of SA was accurately judged. Levels of actual control at 50% or higher were rated with a bias toward greater control, while lesser levels (e.g., 25%) were rated below actual levels. The sigmoidal relationship between SA and the actual level of control reflects that the brain does not present an accurate perception of control to consciousness. One possible explanation is that the neural process of SA perception biases the accurate nonconscious determination of control, possibly carried out by the comparator. This intrinsic bias serves to balance the need for greater accuracy with the additional processing time required to make a reasonable prediction.(Synofzik et al. 2006) An alternate hypothesis is that biased SA is a consequence of an inaccurate nonconscious detection of control, and underlying neural processes are only optimized to detect full control or no control. Despite suggestions that the explicit judgment and implicit processing of SA are 2 distinct cognitive processes, the critical early attention-independent mechanisms for mismatch detection and SA judgment that precede awareness are likely the same.

The results of the fMRI experiment yielded information about the neural correlates of the implicit processing of SA, the differential responsivity of these brain regions during various levels of mismatch, and the connectivity of the complete network. The LTM method identified numerous brain regions previously implicated in the processing of SA, including the PPC (Fink et al. 1999; Farrer and Frith 2002; Farrer et al. 2003), STS (Leube et al. 2003), DLPFC (Fink et al. 1999), pre-SMA (Farrer et al. 2003), precuneus (Farrer and Frith 2002), insula (Farrer et al. 2003; Karnath et al. 2005; Brass and Haggard 2007; Klein et al. 2007), and cerebellum (Fink et al. 1999). Both the PPC and the cerebellum have been implicated in the processing of visual and motor prediction and detection of incongruence (Blakemore and Sirigu 2003). STS has previously been shown to respond differentially to visual-motor incongruence during self-generated movement, though this region is also known to be a key area in the mirror neuron network (Leube et al. 2003). DLPFC has been implicated in conflict between intention and sensory feedback (Fink et al. 1999). SMA or pre-SMA and the insula are hypothesized to contribute to the phenomenon of intentional binding, where motor intention is

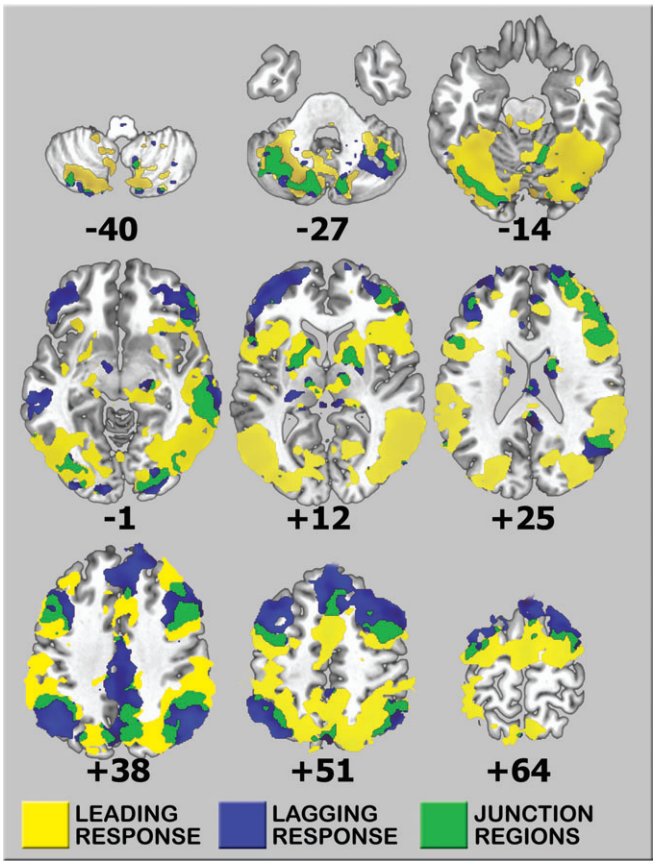

Figure 6. Functional connectivity analysis utilizing seeds from the loss-responsive regions. Leading (yellow) and lagging (blue) response regions demonstrate separate functional networks that are internally coherent. Additional relay regions (green) that are anatomically intermediate to the leading and lagging networks demonstrate high correlation values to both networks.

matched up with sensory feedback. More recently, however, Desmurget et al. (2009) used electrical stimulation to target the various SA brain regions to assess the subjective perceptions associated with each area. Stimulation of PPC led subjects to report an intention to move and even the perception of movement in the absence of actual movement by EMG (Desmurget et al. 2009). This led the authors to hypothesize that both conscious intention and motor awareness, the perception that an intended action was being executed, arose in the PPC.

Moving beyond the LTM regions to the raw BOLD-response time courses, we found a striking consistency across all of the loss-responsive regions showing a stratification in BOLD-response amplitudes, ranging from 0% to 100% control. These small amplitude differences across the % control conditions may represent actual changes in the magnitude of the BOLD response, reflecting the larger amplitudes of more demanding tasks. An alternate explanation is that they reflect the time required to process the level of mismatch, which cannot be adequately sampled due to the limited temporal resolution of fMRI. For example, a more complex cognitive task will induce a slightly longer blood flow response than a simpler task, yet the limitations of sampling the blood flow every 2-s and the prolonged nature of the hemodynamic response would lead to similar response profiles, with only subtle differences in amplitude. Regardless of the explanation, these findings demonstrate a broad neural network with the ability to monitor and relay mismatch in each region. Furthermore, these findings show that full control and SA are the default, with the regions and networks we identified only becoming proportionally responsive during the loss of control.

Although the stratification based on the level of mismatch may suggest that each of these loss-responsive regions may serve as a separate comparator, the connectivity analysis suggests that the time courses may reflect a spatially and temporally defined information flow. This hypothesis is supported by several observations from the data. First, the loss-responsive regions all demonstrate one of 2 possible temporal activity profiles. These 2 temporal profiles suggest a directionality of information flow going from leading-response areas to lagging-response areas based on the later time to peak of the lagging response. Second, the regions comprising the leading or lagging networks are more internally connected to each other than to areas in the other network independent of proximity. Lastly, a small number of "junction" regions, located at the interface of leading and lagging areas, appear to serve as relays based on their intermediate connectivity to the 2 response networks.

Based on our proposed model of information flow during the processing of SA, the leading network is likely to be involved in mismatch detection led primarily by the right supramarginal gyrus, left anterior IPL, anterior insula, and right temporoparietal junction. The mismatch information then moves to the anatomically intermediate relays, before being transmitted to the lagging network. The lagging network is comprised mainly of bilateral prefrontal, cingulate, and bilateral posterior IPL. The involvement of the prefrontal cortex in the lagging network provides indirect evidence of this network's later role in the processing of SA. These findings are also likely to explain why stimulation of the PPC may lead to the perception of intention and the impression of movement since this region not only receives the efference copy of the intended movement, but then transmits the "match" signal downstream to the prefrontal cortex where SA is consciously experienced.

We did not identify any brain regions that responded similarly to the bias effect we noted on the behavioral testing. This was attempted by using the individual subject ratings of control from the behavioral experiment, though the inherent limitations of this method are obvious since subjects may have experienced different levels of control over time. Alternatively, any attempts to combine implicit processing and explicit judgment would be nondissociable. Other explanations for this finding include the inability of a rapid binary judgment to be detected by BOLD fMRI or that the explicit judgment and implicit processing of SA are indeed mediated by different brain mechanisms. Future studies utilizing imaging methodologies with higher temporal resolution than fMRI may help to determine the significance of the leading and lagging networks we identified. Furthermore, the study of patients with disorders of volition (e.g., schizophrenia, alien limb phenomena, psychogenic movement disorders, or phantom limb) with impaired SA can also provide additional answers regarding the neural correlates of bias and clarify the roles played by the various regions in this complex SA network.

Funding

Intramural program of the National Institute of Neurological Disorders and Stroke.

Notes

Conflict of Interest: None declared.

References

Blakemore SJ, Sirigu A. 2003. Action prediction in the cerebellum and in the parietal lobe. Exp Brain Res. 53:239–245.

Brass M, Haggard P. 2007. To do or not to do: the neural signature of self-control. J Neurosci. 27:9141–9145.

Cohen MS. 1997. Parametric analysis of fMRI data using linear systems methods. Neuroimage. 6:93–103.

Costantini M, Haggard P. 2007. The rubber hand illusion: sensitivity and reference frame for body ownership. Conscious Cogn. 16:229–240.

Cox RW. 1996. AFNI: Software for analysis and visualization of functional magnetic resonance neuroimages. Computers and Biomedical Research. 29:162–173.

David N, Cohen MX, Newen A, Bewernick BH, Shah NJ, Fink GR, Vogeley K. 2007. The extrastriate cortex distinguishes between the consequences of one's own and others' behavior. Neuroimage. 36:1004–1014.

David N, Newen A, Vogeley K. 2008. The "sense of agency" and its underlying cognitive and neural mechanisms. Conscious Cogn. 17:523–534.

Desmurget M, Reilly KT, Richard N, Szathmari A, Mottolese C, Sirigu A. 2009. Movement intention after parietal cortex stimulation in humans. Science. 324:811–813.

Ehrsson HH, Spence C, Passingham RE. 2004. That's my hand! Activity in premotor cortex reflects feeling of ownership of a limb. Science. 305:875–877.

Farrer C, Franck N, Georgieff N, Frith CD, Decety J, Jeannerod M. 2003. Modulating the experience of agency: a positron emission tomography study. Neuroimage. 18:324–333.

Farrer C, Frith CD. 2002. Experiencing oneself vs another person as being the cause of an action: the neural correlates of the experience of agency. Neuroimage. 15:596–603.

Fink GR, Marshall JC, Halligan PW, Frith CD, Driver J, Frackowiak RS, Dolan RJ. 1999. The neural consequences of conflict between intention and the senses. Brain. 122:497–512.

Forman SD, Cohen JD, Fitzgerald M, Eddy WF, Mintun MA, Noll DC. 1995. Improved assessment of significant activation in functional magnetic resonance imaging (fMRI): use of a cluster-size threshold. Magn Reson Med. 33:636–647.

Friedman J, Flash T. 2007. Task-dependent selection of grasp kinematics and stiffness in human object manipulation. Cortex. 43:444–460.

Frith CD. 1992. The cognitive neuropsychology of schizophrenia. Hove (UK): Lawrence Erlbaum.

Frith CD, Blakemore SJ, Wolpert DM. 2000. Abnormalities in the awareness and control of action. Philos Trans R Soc Lond B Biol Sci. 355:1771–1788.

Gallagher S. 2000. Philosophical conceptions of the self: implications for cognitive science. Trends Cogn Sci. 4:14–21.

Haggard P, Magno E. 1999. Localising awareness of action with transcranial magnetic stimulation. Exp Brain Res. 127:102–107.

James W. 1890. The principles of psychology. New York: Dover Publications.

Jeannerod M. 1997. The cognitive neuropsychology of action. Oxford: Blackwell.

Karnath HO, Baier B, Nagele T. 2005. Awareness of the functioning of one's own limbs mediated by the insular cortex? J Neurosci. 25:7134–7138.

Klein TA, Endrass T, Kathmann N, Neumann J, von Cramon DY, Ullsperger M. 2007. Neural correlates of error awareness. Neuroimage. 34:1774–1781.

Leube DT, Knoblich G, Erb M, Grodd W, Bartels M, Kircher TT. 2003. The neural correlates of perceiving one's own movements. Neuroimage. 20:2084–2090.

Repp BH, Knoblich G. 2007. Toward a psychophysics of agency: detecting gain and loss of control over auditory action effects. J Exp Psychol. 33:469–482.

Saad ZS, Chen G, Reynolds RC, Christidis PP, Hammett KR, Bellgowan PS, Cox RW. 2006. Functional imaging analysis contest (FIAC) analysis according to AFNI and SUMA. Hum Brain Mapp. 27:417–424.

Sirigu A, Daprati E, Ciancia S, Giraux P, Nighoghossian N, Posada A, Haggard P. 2004. Altered awareness of voluntary action after damage to the parietal cortex. Nat Neurosci. 7:80–84.

Sirigu A, Daprati E, Pradat-Diehl P, Franck N, Jeannerod M. 1999. Perception of self-generated movement following left parietal lesion. Brain. 122:1867–1874.

Slachevsky A, Pillon B, Fourneret P, Pradat-Diehl P, Jeannerod M, Dubois B. 2001. Preserved adjustment but impaired awareness in a sensory-motor conflict following prefrontal lesions. J Cogn Neurosci. 13:332–340.

Sperry RW. 1950. Neural basis of the spontaneous optokinetic response produced by visual inversion. J Comp Physiol Psychol. 43:482–489.

Synofzik M, Their P, Lindner A. 2006. Internalizing agency of self-action: perception of one's own hand movements depends on an adaptable prediction about the sensory action outcome. J Neurophysiol. 96:1592–1601.

Synofzik M, Vosgerau G, Newen A. 2008. Beyond the comparator model: a multifactorial two-step account of agency. Conscious Cogn. 17:219–239.

Von Holst E. 1954. Relations between the central nervous system and the peripheral organs. Br J Anim Behav. 2:89–94.

Wegner DM, Sparrow B, Winerman L. 2004. Vicarious agency: experiencing control over the movements of others. J Pers Soc Psychol. 86:838–848.